Evaluating the Structure of Catalysts Using Core-Level Binding Energies Calculated from First Principles

Quang Thang Trinh,[†] Kong Fei Tan,[†] Armando Borgna,[‡] and Mark Saeys*,[†]

[†]Department of Chemical and Biomolecular Engineering, National University of Singapore, 4 Engineering Drive 4, Singapore 117576

[‡]Institute of Chemical and Engineering Sciences, 1 Pesek Road, Singapore 627833

Supporting Information

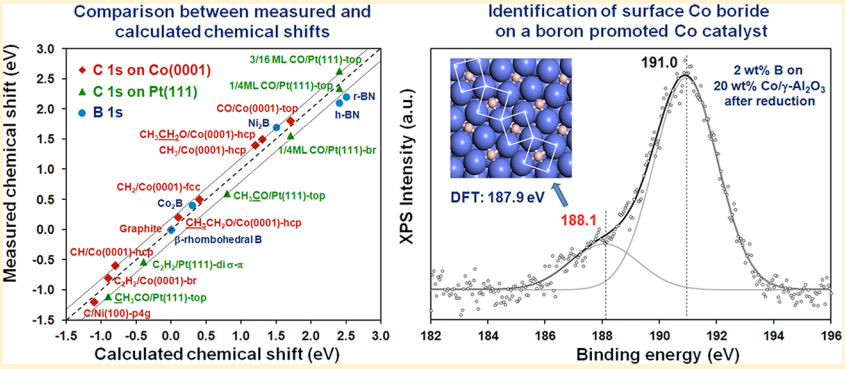

ABSTRACT: X-ray photoelectron spectroscopy (XPS) is a powerful and popular surface characterization technique, and the measured shifts in the core electron binding energies are sensitive to the chemical structure and local environment of the surface species. C 1s binding energies were calculated with density functional theory (DFT) for 17 structures including eight well-characterized structures on a Co(0001) surface and nine on a Pt(111) surface, while B 1s binding energies were calculated for six well-characterized structures and compared with experimental values. DFT calculations describe the 2.8 eV variation in the C 1s binding energies on Co surfaces, the 4.2 eV variation in the C 1s binding energies on Pt surfaces, and the 5.5 eV variation in the B 1s binding energies in the test sets with average deviations of 85, 73, and 53 meV, respectively. The shift in the C 1s and the B 1s binding energies can be correlated with the calculated charges, though only within homologous series. To illustrate how binding energy calculations can help elucidate catalyst structures, the nature of the resilient carbon species deposited during Fischer–Tropsch synthesis (FTS) over Co/γ-Al_2O_3 catalysts was studied. The catalysts were investigated using XPS after reaction, and the measured C 1s binding energies were compared with DFT calculations for various stable structures. The XPS peak at 283.0 eV is attributed to a surface carbide, while the peak at 284.6 eV is proposed to correspond to remaining waxes or polyaromatic carbon species. Boron promotion has been reported to enhance the stability of Co FTS catalysts. Again, the combination of XPS with DFT B 1s binding energy calculations helped identify the nature and location of the boron promoter on the Co/γ-Al_2O_3 catalyst.

1. INTRODUCTION

Since its introduction in 1958,[1] X-ray photoelectron spectroscopy (XPS) or electron spectroscopy for chemical analysis (ESCA) has become a popular surface characterization technique in heterogeneous catalysis.[2,3] In XPS, a core-level electron is excited by X-rays, and the kinetic energy of the collected electrons is measured. From an energy balance, the binding energy (BE) of the core-level electrons can be determined. It has been found that core-level BEs are highly sensitive to the chemical state and the environment of the surface species, and the chemical shift in the BEs can be used to identify the structure and the binding site of the surface species. Moreover, the relatively small penetration depth of the photoelectrons makes XPS surface sensitive.[4] The introduction of synchrotron-based XPS has reduced acquisition times to a few milliseconds per spectrum and enhanced the energy resolution to better than 0.1 eV.[5] In addition, depth-profile measurements[6,7] and *in situ* studies[8,9] have recently appeared. With those improved measurement techniques, modeling-based analysis tools become important to help interpret the spectra.

Chemical shifts in the core-level BEs have been interpreted as initial-state effects originating from changes in the electrostatic interactions between the core electrons and the valence electrons and final-state effects arising from charge rearrangement and relaxation occurring in response to the core hole.[10−12] Initial-state effects dominate the chemical shifts in many cases; however, final-state effects are not always negligible and may contribute positively or negatively.[10,12,13] Various factors that contribute to initial-state chemical shifts were discussed in by Methfessel and Fiorentini[13] and by Weinert and

Received: September 10, 2012
Revised: December 10, 2012

Watson[14] and include interatomic charge transfer, changes in the reference Fermi-energy level, intra-atomic charge transfer, charge transfer from the local environment to the atom, and redistribution of charge due to bonding and hybridization. Charge transfer is hence often invoked to interpret shifts in the core-level BEs.[11−16] Chemical shifts are found to correlate quite well with charges for gas-phase molecules[11] and for some bimetallic systems,[13,16] but the correlation has been debated for bulk alloys and for adlayer systems.[14] In practice, chemical shifts result from a complex combination of various factors, which often partially cancel.[12−14] This makes it challenging to quantitatively interpret chemical shifts.

Density functional theory (DFT) has become an important tool to analyze heterogeneous catalytic reactions.[17,18] In particular, the relative stability of various possible reaction intermediates and the activation barriers of surface reactions are calculated routinely. In addition, calculated vibration spectra can help identify the structure and the adsorption site of surface species [e.g., refs 19−21]. Chemical shifts have also been calculated from first principles.[10,12−15,22−25] For example, Takahata and Chong[23] calculated core-level BEs for a test set of 59 small gas-phase molecules with an average deviation of 160 meV. Core-level BE calculations have been used to analyze the surface structure and the nature of the surface species in catalysis. For example, Todorova et al.[24] identified the structure of a strained PdO(101) layer on Pd(100) using DFT calculations in combination with calculated O 1s BEs and scanning tunneling microscopy images. Bianchettin et al.[25] combined synchrotron-based XPS with calculated Rh $3d_{5/2}$ surface core-level shifts to investigate the Rh(100) surface reconstruction induced by oxygen. Kresse and Kohler[10] compared calculated vibration frequencies and Rh $3d_{5/2}$ surface core-level shifts with experimental values to confirm the preferred top adsorption site of CO on Rh(111). With the development of fast and high-resolution synchrotron-based XPS techniques, calculated chemical shifts are expected to become an important tool to analyze surface species and surface structures.

In this paper, we demonstrate that C 1s and B 1s chemical shifts can be calculated accurately using DFT with the final-state approximation. Next, we illustrate how such calculations, in combination with thermodynamic stability calculations, can help identify the nature of the resilient carbon species that are formed on a Co/γ-Al_2O_3 catalyst during Fischer−Tropsch Synthesis (FTS)[26] and help elucidate the chemical state and the location of the boron promoter that was found to enhance the stability of Co catalysts.[27]

2. COMPUTATIONAL AND EXPERIMENTAL METHODS

Computational Methods. All structures were optimized using periodic spin-polarized DFT with the Perdew−Burke−Ernzerhof functional (DFT-PBE)[28] as implemented in the Vienna ab initio simulation package (VASP).[29,30] Plane waves with a kinetic energy up to 450 eV were used, and the electron−ion interactions were described by the projector-augmented wave (PAW) method.[31,32] The structures were optimized using a conjugate-gradient method until the atomic forces were less than 0.01 eV/Å. A second-order Methfessel−Paxton scheme with a 0.2 eV smearing width was used to facilitate the convergence of the electronic structure, and the energy convergence for the electronic structure was set to 10^{-4} eV. C 1s BEs were computed for several structures. All the optimized structures and the calculated core-level BEs are shown in the Supporting Information. We focused our study on closed-packed Pt(111) and Co(0001) surfaces because they are the dominant facets for catalyst particles and because most experimental XPS literature is available for closed-packed surfaces. On Co(0001), the following species were considered for a 1/9 ML coverage (the experimental references are indicated for each structure): CH_3CH_2O at the hcp hollow site[33] and, for comparison, at the less-preferred top site, C_2H_2 across the bridge site with C in neighboring hollow sites,[34] CH at the hcp hollow site,[35] CH_2 at the hcp hollow site,[35] CH_3 at the hcp hollow[35] and at the less-preferred top site, a graphene overlayer centered at the bridge sites, CCH_3 at the hcp hollow site, and carbon atoms at the subsurface octahedral sites, and CO at the top[36] and at the hcp hollow site for a 1/3 ML coverage. In addition, carbon adsorption at the B5 step sites and a surface p4g clock carbide growing from the step edge[26] were calculated. To include a C 1s core-level BE for a surface p4g clock carbide in the test set, the p4g clock reconstruction induced by carbon on Ni(100)[12] was included. Orthorhombic bulk cobalt carbide (Co_2C) with optimized lattice parameters of 2.92, 4.48, and 4.42 Å was also evaluated. Graphite was modeled using the experimental lattice.[37] On Pt(111), C 1s BEs were calculated for the following species for a coverage of 1/9 ML: CH_3CH_2OH and CH_3CO, both at the top site,[38] two configurations of CH_3CHO (η^1(O) with O at a top site, and η^2(C,O) with C═O over a bridge site[39]), and CH_3 at the top site.[40] Di-σ−π adsorbed C_2H_2,[41] di-σ adsorbed and π-adsorbed C_2H_4[41,42] and CCH_3 at the fcc hollow site[42,43] were considered for a 1/4 ML saturation coverage. Two structures were considered for CO: 1/2 ML with CO at both top and bridge sites in a $p(4 \times 2)$ unit cell[43,44] and a lower 3/16 ML coverage with CO at the top sites in a $p(4 \times 4)$ unit cell.[43] For the B 1s BEs, the following structures were considered: β-rhombohedral boron[45] with an experimental lattice parameter of 10.13 Å and angle of 65.2°, tetragonal Co_2B[46] with optimized lattice parameters of 4.98 and 4.28 Å, tetragonal Ni_2B[47] with optimized lattice parameters of 4.99 and 4.28 Å, rhombohedral-BN[48] with experimental lattice parameters of 2.50 and 9.99 Å, hexagonal-BN[49] with experimental lattice parameters of 2.50 and 6.66 Å, cubic-BN[49] with an optimized lattice parameter of 3.58 Å, and B_2O_3[45] with optimized lattice parameters of 4.36 and 8.39 Å. In addition, a surface Co p4g clock boride growing from the step edges, boron at the B5 step sites, subsurface boron, and adsorbed BH with coverage of 1/9 ML at the hcp hollow site were included.

Hcp Co(0001), fcc Pt(111), and fcc Ni(100) surfaces were modeled as three-layer slabs, where the bottom layer was fixed at the optimized bulk lattice parameters of 2.49, 3.98, and 3.52 Å, respectively. Co step sites were created by removing two rows of Co atoms from the top layer of a $p(2 \times 8)$ hcp Co(0001) slab.[26] A $(5 \times 5 \times 1)$ Monkhorst−Pack k-point grid was used to sample the Brillouin zone for $p(3 \times 3)$ unit cells, while a $(5 \times 2 \times 1)$ grid was used for larger $p(2 \times 8)$ unit cells and a $(3 \times 3 \times 1)$ grid for $p(4 \times 4)$ unit cells. Repeated slabs were separated by 12 Å to minimize interactions between slabs. Adsorption energies were converged within 5 kJ/mol with respect to the vacuum spacing and the k-point sampling. Increasing the slab thickness from 3 to 5 layers reduced the carbon adsorption energy at the hollow site on Co(0001) by 7 kJ/mol and the boron adsorption energy by 5 kJ/mol, while the C 1s and B 1s BEs changed by less than 60 meV for adsorbed CH_x and BH species. Also for Pt(111), increasing the slab thickness to five layers changed C 1s BEs for C_2H_5OH,

CH_3CO, C_2H_2, C_2H_4, and CCH_3 by less than 100 meV. Therefore, we only report results for the three-layer calculations.

Core-Level Binding Energy Calculations. In XPS, a core electron is excited by a beam of photons to create a core hole. The measured core-level BE is the energy difference between the initial, unexcited ground-state and the final, core-excited state. Several schemes have been developed to calculate core-level BEs using DFT (for example, see Olovsson et al.[22] for a detailed discussion) and include the initial-state approximation where screening of the core hole in the core-excited state is neglected, the final-state approximation where the core hole is completely screened, and the transition-state model where partial orbital occupation numbers are introduced to describe the excitation process.[10,22] In this work, core-level BEs were calculated with the final-state approximation as implemented in VASP.[10] In the final-state approximation, core-level BEs are calculated as the energy difference between an unexcited ground-state calculation and a core-excited-state calculation in which a specified core electron is removed and an electron is added to the lowest unoccupied valence state to completely screen the localized core hole and preserve the charge neutrality of the system. In the final-state approximation, the resulting core hole is hence completely screened, as indicated by the extra charge in the local valence density of states of the core-excited atom.

Since relative energies are calculated more accurately than absolute BEs, chemical shifts are calculated rather than absolute core-level BEs. Core-level BEs are then obtained using an experimental reference value. Hence, C 1s BEs are calculated using the C 1s BE of graphite, 284.4 eV,[37] as the reference, while the B 1s BE of bulk β-rhombohedral boron, 187.9 eV,[45] was used as the reference for the B 1s BEs. With our settings, the calculated core-level BEs are expected to be numerically converged within 20−50 meV.[10,15] To evaluate the effect of the unit cell size on the calculated core-level BE, we calculated the C 1s core-level BE for 1 ML atop CO on Pt(111) by exciting one C 1s electron in a $p(2 \times 2)$ and in a $p(3 \times 3)$ unit cell. The calculated C 1s BE was found to increase by less than 20 meV when the unit cell size was increased. Finally, Bader charges[50,51] were computed to evaluate the correlation between the calculated charge transfer and the core-level BEs.[11−16]

Experimental Methods. To illustrate how calculated chemical shifts can help elucidate catalyst structures, we studied the nature of resilient carbon species formed on Co catalysts during FTS and the nature and possible location of a boron promoter on this catalyst. Co/γ-Al_2O_3 catalysts were prepared by slurry impregnation of a γ-Al_2O_3 support with an aqueous Co nitrate solution, $Co(NO_3)_2 \cdot 6H_2O$, as described by Tan et al.[26] The Co catalysts were tested during FTS, the conversion of synthesis gas to long chain hydrocarbons, for 200 h in a fixed bed microreactor.[26] After 200 h, the reactor temperature was reduced, and the catalyst was removed for characterization without exposure to air. The nature of the resilient carbon species remaining on the Co catalyst after careful wax extraction with hexane was studied with XPS. XPS spectra were obtained using a Thermo ESCALAB 250 spectrometer with a monochromatic aluminum anode (Al Kα = 1487 eV) and a 500 mm Rowland circle monochromator to produce a small X-ray spot with a minimum energy spread. Measurements were recorded for a 20 eV pass energy, a 0.1 eV kinetic energy step, and a 0.1 s dwelling time. Energy corrections used the Al 2p peak of the γ-Al_2O_3 support at 74.3 eV. Promotion with small amounts of boron was found to increase stability of Co catalyst during FTS.[27] To improve the B 1s XPS signal-to-noise ratio, 2.0 wt % boron was introduced to the Co/γ-Al_2O_3 in second slurry impregnation step using aqueous boric acid (H_3BO_3).[27] After reduction in flowing H_2 at 500 °C for 2 h, the catalysts were purged with Ar and cooled to room temperature. Then, the catalysts were characterized by XPS.

3. RESULTS AND DISCUSSION

First, C 1s BE calculations are evaluated for a range of species adsorbed on Co(0001) and Pt(111). Next, B 1s BEs are calculated for several well-characterized materials. Finally, core-level BE calculations are used to help identify the nature of resilient carbon species formed during FTS and the location and nature of the boron promoter introduced to enhance the stability of Co catalysts during FTS.

C 1s Binding Energies for Species on Co(0001). Experimental C 1s BEs are compared with calculated BEs in Figure 1a. In general, the final-state DFT-PBE calculations capture the 2.8 eV variation in the experimental BEs well when going from a p4g clock carbide to CO at a top site of Co(0001). Deviations between experimental C 1s XPS positions and calculated core-level BEs are typically smaller than 100 meV, and the average deviation is 85 meV. The largest deviation is found with the synchrotron-based XPS data for CH_3CH_2O on Co(0001); however, the difference between the calculated CH_2 and CH_3 C 1s BEs of 285.72 and 284.50 eV, respectively, corresponds well with the difference between the experimental peaks at 285.9 and 284.6 eV. These deviations should be compared with a typical energy resolution of about 0.5 eV in standard XPS and of about 0.1 eV in synchrotron-based XPS.[5]

To analyze the effect of charge transfer on the variation in the core-level BEs over the test set, the net Bader charges on the carbon atoms are plotted against the calculated C 1s BEs in Figure 1b. As discussed in the literature, charge transfer is often invoked to analyze chemical shifts.[11−16] Withdrawal of valence electrons reduces the screening of the nuclear charge by the valence electrons and hence increases the core-level BEs. However, other factors such as hybridization and local dipole moments also affect the chemical shift,[12−14] and the correlation in Figure 1b seems valid only within homologous series at similar sites. Indeed, the correlation in Figure 1b is at best qualitative with a R^2 value of 0.59. In particular, when moving from one adsorption site to another, the change in core-level BE is often smaller than expected from the change in the Bader charge, suggesting that the change in hybridization is an important factor as well. The low C 1s BE for p4g carbon on Ni(100) is found to correspond with the transfer of nearly one electron from the surrounding Ni atoms to the p4g clock carbon atom, as also discussed by Martensson and Nilsson.[12] A similar charge transfer was calculated for a p4g clock carbide formed near the edge sites of Co terraces.[26] Also for C_2H_2, the low C 1s BE correlates with strong backdonation from Co(0001) to adsorbed ethyne. Within the CH_x series, the variation in the core-level BE correlates with the carbon charge, though the variation in the BEs is somewhat larger than expected from the overall correlation.

To evaluate the sensitivity of the calculated C 1s BEs to the adsorption site, CO at the hcp hollow site, CH_3 at the top site, and CH_3CH_2O at the top site were also considered. The calculated C 1s BE decreases from 286.1 to 285.6 eV when CO is moved from the top to the hcp site, and the calculated C 1s

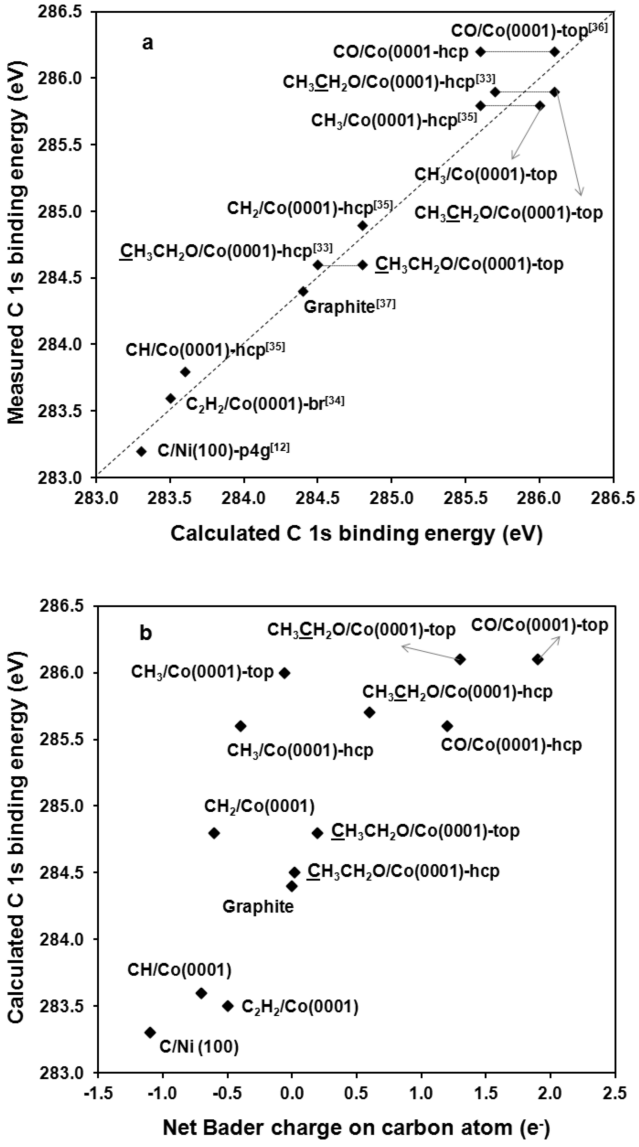

Figure 1. (a) Calculated and experimental C 1s binding energies for various well-characterized carbon species on Co(0001) and Ni(100). The adsorption site and the experimental reference are indicated. (b) Correlation between the net Bader charge on the carbon atom and the calculated C 1s binding energy.

BE for CO at the hollow site does not agree with the experimental value of 286.2 eV for a low CO coverage. The decrease in core-level BE correlates with the lower positive Bader charge on the carbon atom, which is in turn consistent with the enhanced backdonation from the Co d-band to the CO $2\pi^*$ orbitals at the hollow site. CH_3 is 46 kJ/mol less stable at the top site than at the hcp site on Co(0001), in agreement with other theoretical studies.[52] The calculated C 1s BE increases from 285.6 to 286.0 eV when CH_3 is moved from the hcp site to the top site. The increase in core-level BE correlates with a decrease in the charge density on the carbon atom. CH_3CH_2O binds 71 kJ/mol stronger at the hcp site than at the top site. The change in adsorption site increases the C 1s BE of the CH_2 group by 0.5 eV and of the CH_3 group slightly less by 0.3 eV. In particular for the CH_3 group, the agreement with the experimental value worsens. The increase in the core-level BE is correlated with a decrease in the Bader charge. However, for the CH_2 group the decrease in the Bader charge, 0.7*e*, is larger than expected from the increase in the C 1s BE, and other factors again affect the shift in the CH_2 C 1s BE.

C 1s Binding Energies for Species on Pt(111). To confirm the accuracy of the C 1s BE calculations for other surfaces, we considered several well-characterized hydrocarbon species on a closed-packed Pt(111) surface. C 1s BE calculations for nine structures are compared with experimental data in Figure 2a. The final-state DFT calculations capture the

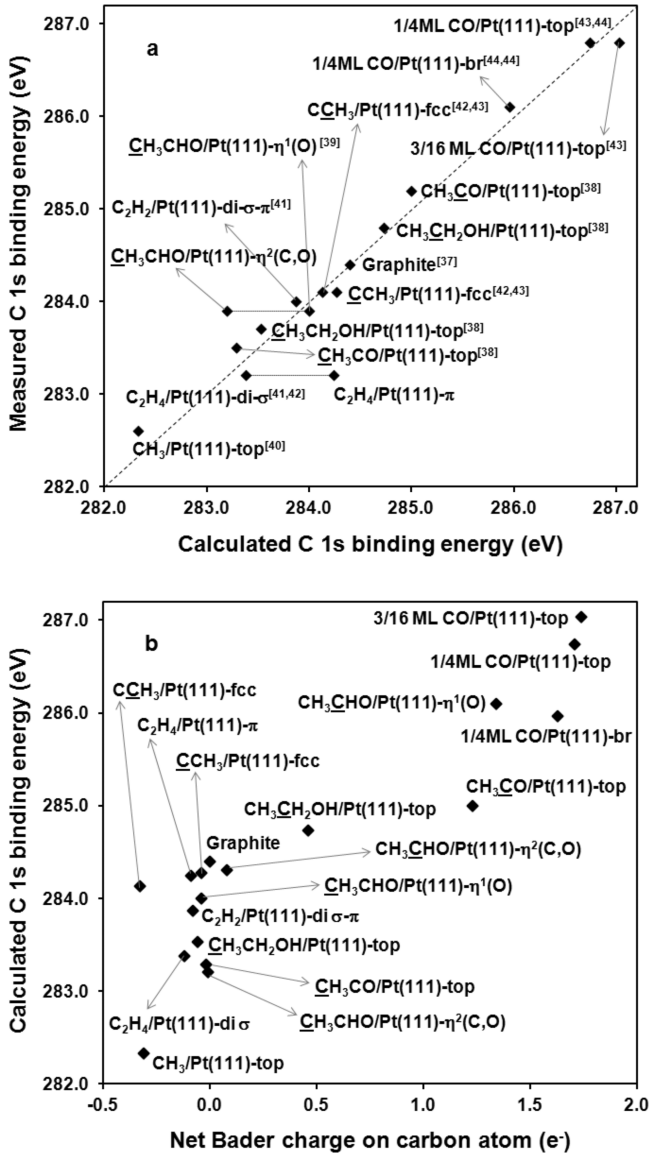

Figure 2. (a) Calculated and experimental C 1s binding energies for various well-characterized carbon species on Pt(111). The adsorption site and the experimental reference are indicated. (b) Correlation between the net Bader charge on the carbon atom and the calculated C 1s binding energy.

4.2 eV variation in the C 1s BEs for the test set, ranging from CH_3 at the top site to CO at top sites, with an average deviation of 73 meV. The largest deviation is for CH_3 at the top site, where the calculations underestimate the BE by 270 meV, to be compared with a typical conventional XPS resolution of about 0.5 eV.

When there are multiple carbon atoms in the structure, they can be difficult to distinguish by conventional XPS. For a low

ethanol coverage on Pt(111), synchrotron-based XPS was able to distinguish the CH_2 and CH_3 groups, with peaks at 284.8 and 283.7 eV, respectively,[38] while a single peak was reported in an earlier conventional XPS study.[39] Both the position and the difference in the measured BEs are in good agreement with the calculated values of 284.7 and 283.5 eV, respectively. Also for CH_3CO, two peaks at 285.2 and 283.5 eV are separated by synchrotron-based XPS,[38] and both compare well with the calculated values, 285.1 and 283.3 eV. In a conventional XPS study, only a single C 1s peak at 283.9 eV was observed for acetaldehyde on Pt(111), and this peak was assigned to CH_3.[39] Two stable configurations are found for acetaldehyde on Pt(111): η^1(O) (top) and η^2(C,O) (di-σ) (Supporting Information) with a DFT-PBE adsorption energy difference of only 4 kJ/mol. The calculated C 1s BEs for the CHO and CH_3 group in the η^2(C,O) configuration are 284.5 and 283.2 eV, respectively, and 286.1 and 284.0 eV, respectively, in the η^1(O) configuration. The calculated CH_3 C 1s BE for the η^1(O) configuration agrees with the experimental value of 283.9 eV, while the calculated BEs for the η^2(C,O) configuration differ somewhat more. This is consistent with the dominant η^1(O) configuration that has been observed in surface science studies.[53] An important species during hydrogenation and dehydrogenation reactions on Pt is CCH_3. Both synchrotron-based and conventional XPS studies find a single C 1s peak at 284.1 eV for CCH_3 on Pt(111), and the two carbon atoms could not be distinguished.[42,43] This is consistent with the very small difference in the calculated C 1s BEs of 284.27 and 284.13 eV. Note that for CCH_3 on Co(0001) the difference in the C 1s BEs is much larger at 1.0 eV (Table 1).

Also on Pt(111), the calculated C 1s BEs are sensitive to the adsorption site. For a high 1/2 ML coverage, CO occupies both the top and the bridge sites in a $p(4 \times 2)$ unit cell (Supporting Information), as shown by low-energy electron diffraction (LEED)[43] and by photoelectron diffraction (PED) studies.[44] In synchrotron-based XPS, two C 1s peaks are distinguished at 286.8 and 286.1 eV for this structure. The calculated C 1s BEs of 286.74 eV for CO-top and 285.96 eV for CO-bridge agree well with the experimental values. At a lower coverage, CO occupies only top sites on Pt(111). In particular, for a 3/16 ML coverage, a C 1s BE of 286.8 eV was measured by conventional XPS,[43] in reasonable agreement with the calculated value of 287.03 eV. Two adsorption geometries have been reported for C_2H_4 on Pt(111), di-σ and π. Though di-σ adsorption is the most stable structure in the DFT-PBE calculations, both structures have been identified by high-resolution electron energy loss spectroscopy (HREELS) and temperature-programmed desorption (TPD) studies.[54] The calculated C 1s BE for di-σ C_2H_4, 283.38 eV, matches both the 283.2 eV peak determined by synchrotron-based XPS[42] and the 283.4 eV peak determined by conventional XPS for a 1/4 ML C_2H_4 coverage.[41] The calculated C 1s BE for π-adsorbed C_2H_4, 284.24 eV, does not agree well with those experimental values.

The Bader charges on the carbon atoms are plotted against the calculated C 1s BEs in Figure 2b. The chemical shifts and the charges show similar trends, and the correlation is somewhat better than for hydrocarbon species on Co(0001), with a R^2 value of 0.83 (Figure 1b). The lowest C 1s BE in the test set, CH_3 on Pt(111), corresponds with the most negative charge, −0.3. Similarly to Co(0001), there is significant backdonation to the CH_3 group, but most charge remains on the carbon atom rather than flow to the C−H antibonding orbital. Therefore, the carbon atom is more negative for CH_3 on Pt(111) than for CH_3 on Co(0001). For unsaturated hydrocarbons such as C_2H_4 and C_2H_2 there is net charge transfer to Pt(111), as also reported by Toulhoat et al.,[55] but charge transfer from the H atoms to the C atoms still results in a slightly negative charge on the C atoms. For CCH_3, the charges on the C atoms are quite different (0.3e), yet the two C 1s BEs are very similar, again illustrating that charge transfer is not the only factor determining the core-level shift, and detailed calculations are needed to correctly interpret measured chemical shifts.

Table 1. Calculated Stability under Fischer−Tropsch Conditions, ΔG_r (500 K, 20 bar), and C 1s and B 1s Binding Energy for Various Carbon and Boron Species on Co Surfaces

	Graphene	p4g carbide	CH at hcp	CCH_3 at hcp
Structure	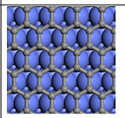	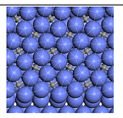	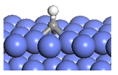	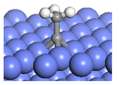
Calculated C 1s BE	284.5	283.3	283.6	284.1 (C) 285.1 (CH_3)
Stability[a]	−116	−98	−72	−90
	Subsurface carbon	Bulk carbide (Co_2C)	Carbon at B5 step	p4g boride
Structure	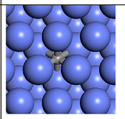	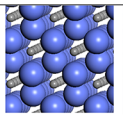	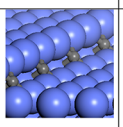	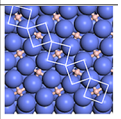
Calculated C(B) 1s BE	283.9	283.2	284.0	187.9
Stability	−15[a]	+16[a]	−95[a]	−59[b]
	Bulk boride (Co_2B)	Boron at B5 step	Monolayer of subsurface B	BH at hcp
Structure	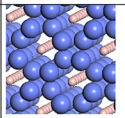	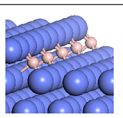	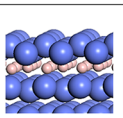	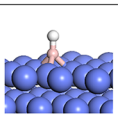
Calculated B 1s BE	188.2	186.5	187.0	186.8
Stability[b]	−29	−27	−53	−24

[a]Gibbs free energy for $CO(g) + (n/2 + 1)H_2(g) \leftrightarrow C_1H_n^* + H_2O(g)$ at typical FTS conditions, 500 K, p_{CO} = 4.4 bar; p_{H_2} = 8.9 bar; p_{H_2O} = 6.7 bar. [b]Gibbs free energy for $^1/_2B_2H_6(g) \leftrightarrow B^* + {}^3/_2H_2(g)$ at 500 K, $p_{B_2H_6}$ = 1.0 bar; p_{H_2} = 8.9 bar.[27,28]

B 1s Core-Level Binding Energies. To evaluate whether accurate core-level BEs can also be calculated for other elements, we included six well-characterized boron species in our test set (Figure 3a). Experimental XPS data for boron compounds are somewhat scarcer than for carbon species, and our test set is more varied than for carbon. In addition, the range in the experimental data for each structure can be rather large; for example, reported B 1s XPS peak positions for B_2O_3 range from 192.0 eV[56] to 193.6 eV.[45] We have therefore selected the experimental values that best agree with our calculated B 1s BEs for Figure 3a. With those data, DFT-PBE calculations describe the 6.0 eV variation in the experimental data with an average deviation of 53 meV. The strongest B 1s BE is calculated for B_2O_3 in our test set, consistent with strong electron withdrawal from the sp_2 boron atoms by the three surrounding oxygen atoms. Boron nitride exists in different crystal structures (Supporting Information). The most stable form is hexagonal-BN. It has a layered structure similar to

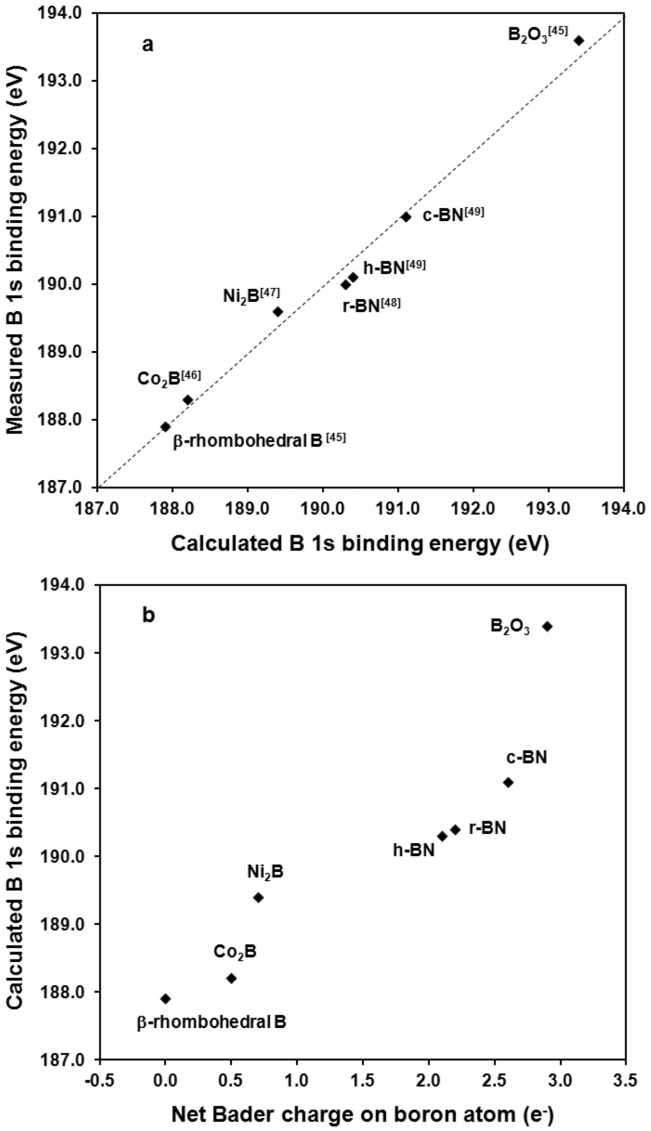

Figure 3. (a) Calculated and experimental B 1s binding energies for various well-characterized bulk boride structure. Experimental references are indicated. (b) Correlation between the net Bader charge on the boron atom and the calculated B 1s binding energy.

graphite, and the boron atoms are sp_2 hybridized. Rhombohedral-BN also has a layered structure, but with a three-layer stacking sequence. It is calculated to be 12 kJ/mol BN less stable than the hexagonal form. The cubic phase, c-BN, has a structure similar to diamond, with sp_3 boron atoms. It is calculated to be 38 kJ/mol BN less stable than h-BN. The relative B 1s BEs for r-BN and h-BN are correctly predicted, and the slightly lower B 1s BE for the more stable r-BN correlates with a more positive Bader charge on the boron atom (Figure 3b). The higher BE in c-BN results from the sp_3 hybridization of the boron atom. Indeed, sp_3 hybridization moves the valence electrons slightly further from the nucleus, leading to reduced screening of the nuclear charge. Finally, two metal borides were considered, Ni_2B and Co_2B. Both display a positive chemical shift relative to bulk boron, as already reported in early XPS studies.[46] The positive shift in tetragonal transition-metal semiborides has been attributed to charge transfer from boron to the transition metal,[57] which is opposite to the charge transfer in transition-metal carbides (Figure 1b).[27] The charge transfer is larger for Ni_2B than for Co_2B, consistent with the higher electronegativity of Ni. The net Bader charges on the boron atoms correlate quite well with the calculated B 1s chemical shifts for this small test set, as shown in Figure 3b.

Identification of Carbon and Boron Species on Supported Co Catalysts by Core-Level BE Calculations. The results in the previous sections suggest that C 1s and B 1s BEs can be calculated by final-state DFT-PBE with accuracies of better than 0.1 eV, which is comparable to the resolution of state-of-the-art synchrotron-based XPS. Moreover, the calculated chemical shifts are sensitive to the chemical state and adsorption site of the boron and carbon species and can hence be used to help identify surface species and catalyst promotors. Next, we illustrate how such calculations, in combination with stability calculations and additional characterization techniques,[26,27] can help identify the nature of the resilient carbon species formed on a supported Co catalyst during FTS and the nature and location of the boron promoter introduced to Co catalysts to improve their long-term stability during FTS.

Supported Co/γ-Al_2O_3 catalysts were tested for 200 h during FTS at 240 °C.[26] Over this period, the catalyst activity decreased by 30%. Based on temperature-programmed hydrogenation (TPH) and transmission electron microscopy (TEM) analysis of the deactivated Co catalysts after 200 h of reaction, the deactivation is attributed, at least in part, to the formation of resilient carbon deposits.[26] The C 1s XPS spectrum for the catalyst after 200 h of reaction and after careful wax extraction is shown in Figure 4a. Deconvolution of the C 1s spectrum suggests the presence of at least two types of resilient carbon species, with C 1s BEs of 282.9 and 284.6 eV, respectively. To help identify those carbon deposits, the thermodynamic stability under FTS conditions and the C 1s BE were calculated for various possible carbon species (Table 1). The most stable

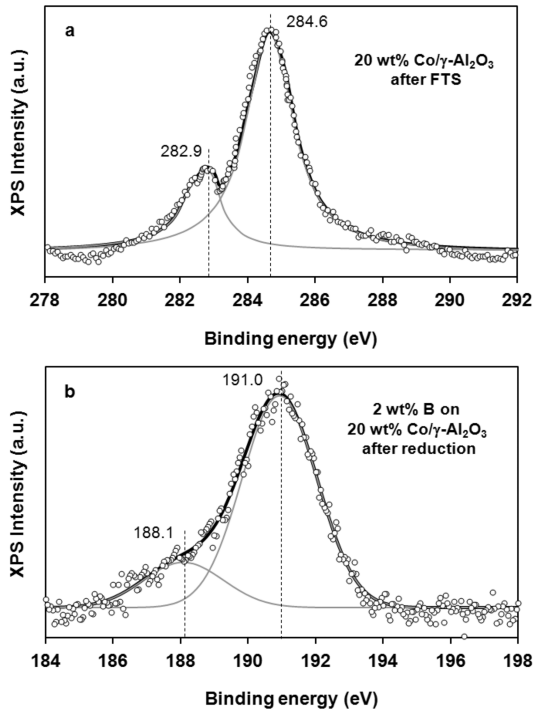

Figure 4. (a) C 1s XPS spectra for a 20 wt % Co/γ-Al_2O_3 catalyst after 200 h of FTS at 20 bar and 240 °C. (b) B 1s XPS spectra for a 20 wt % Co/γ-Al_2O_3 catalyst promoted with 2 wt % boron, after reduction for 12 h in 50 N mL/min H_2 at 500 °C and at atmospheric pressure.

carbon species are an extended polyaromatic graphene overlayer and a p4g surface carbide. Surface hydrocarbon species such as *CH and *CCH_3 are also found to be thermodynamically stable and consistent with the Gibbs free energy of about −105 kJ/mol converted CO for the formation of long chain alkanes from a synthesis gas reservoir during FTS.[26,52] Subsurface carbon and bulk Co carbide (Co_2C) are significantly less stable under these conditions. Based on the calculated C 1s BEs, the peak at 284.6 eV likely corresponds with polyaromatic carbon deposits. However, based on the 285.1 eV binding energy calculated for the CH_3 group in CCH_3, hydrocarbon waxes remaining on the catalyst after careful wax extraction might also contribute to this XPS peak. Note that the C 1s BEs for the two carbon atoms in CCH_3 are quite different on Co(0001), while they were similar on Pt(111) (Figure 2a). This assignment is consistent with the TPH profile and TEM images.[26] The peak at 282.9 eV is attributed to a carbide phase, either a surface carbide or a bulk carbide (Co_2C). A C 1s binding energy of 283.3 eV is calculated for a pg4 clock carbide, while a similar value of 283.2 eV is obtained for a bulk carbide structure. Since thermodynamic calculations show that the formation of a surface carbide is significantly more favorable, the surface carbide structure is the most likely candidate for the XPS peak at 282.9 eV. Note that the 0.4 eV difference is within the range of the resolution of our XPS measurement (Figure 4a).

The addition 0.5 wt % boron to a 20 wt % Co/γ-Al_2O_3 was reported to enhance the catalyst stability during FTS without affecting the maximum activity or selectivity.[27] Indeed, after 200 h of reaction, the boron-promoted Co catalyst retained 95% of its initial activity, while the activity of the unpromoted Co catalyst decreased by 30%. The origin of this increased stability was studied with DFT-PBE.[27] The calculations showed that the presence of a surface cobalt boride near the step edges makes nucleation of carbon at the step edge unfavorable, which prevents nucleation and growth of resilient carbon structure. To investigate the nature of the boron species on the supported Co catalyst, B 1s XPS spectra were collected. The B 1s XPS profile for a Co catalyst promoted with 2.0 wt % boron is shown in Figure 4b. A higher boron loading was used to improve the XPS signal-to-noise ratio. However, the XPS profile for a Co catalyst promoted with 0.5 wt % boron is qualitatively similar.[27] For the catalyst with 2.0 wt % boron, the bulk Co:B atomic ratio determined by inductively coupled plasma-optical emission spectrometry (ICP-OES) differs by less than 5% from the theoretical ratio, 1:0.55. The relative integrated B 1s XPS intensities furthermore show that about 20% of the surface boron species are reduced. In combination with a Co dispersion of 9.5%, a boron coverage of about 1.1 ML on the Co particles can be estimated for this boron loading. Lower boron coverages were obtained for lower boron loadings.[27] Deconvolution of the B 1s spectrum suggests the presence of two boron species, a boron oxide species with a B 1s BE around 191.0 eV, and a reduced form of boron with a B 1s BE around 188.1 eV. The boron oxide species is likely associated with the γ-Al_2O_3 support, since a similar peak was observed when 2.0 wt % boron was introduced to a γ-Al_2O_3 support without Co.[27] Several candidates were considered for the reduced boron species (Table 1). Based on thermodynamic stability calculations, a p4g surface boride and a monolayer of subsurface boron are the most likely candidates. Several BH_x surface species were also considered. BH is the most stable surface species in this family, and BH is 22 kJ/mol more stable than adsorbed BH_3. Surface BH_2 decomposes to BH and surface H during the geometry optimization. A surface boron atom is also thermodynamically unstable under FTS conditions.[27] Since the amount of introduced boron is rather small for the optimal catalyst with 0.5 wt % boron, and a sequential impregnation procedure was followed, the formation of a bulk Co boride (Co_2B) seems unlikely. The calculated B 1s BE for subsurface boron, 187.0 eV, seems too low to correspond with the XPS peak at 188.1 eV. Based on the XPS peak position and the thermodynamic stability, a surface boride is therefore the most likely candidate for the reduced boron species present on the Co/γ-Al_2O_3 catalyst.

4. CONCLUSIONS

X-ray photoelectron spectroscopy (XPS) is a popular surface characterization technique in heterogeneous catalysis. With the development of fast, high-resolution synchrotron-based XPS with *in situ* capabilities, the importance of XPS is expected to increase. In this work, we illustrate that DFT-PBE calculations can help analyze and interpret XPS data. First, final-state DFT-PBE calculations are shown to predict C 1s BEs for 16 well-characterized surface species on Co and Pt with average deviations of 85 and 73 meV, respectively, and B 1s BEs with an average deviation of 53 meV, which can be compared to the 0.1 eV resolution of synchrotron-based XPS and the 0.5 eV resolution of conventional XPS. Our study shows that the accuracy of DFT-PBE core-level BE calculations compares favorably with conventional XPS and could help distinguish chemical shifts when there are multiple types of carbon atoms on the surface, even when they fall within the resolution of conventional XPS. Next, the nature of the resilient carbon deposits formed on a Co/γ-Al_2O_3 catalyst during FTS was analyzed by calculating C 1s BEs and thermodynamic stabilities for various possible candidates. The calculations suggest that polyaromatic carbon islands and a surface carbide are the most likely candidates for the resilient carbon species with XPS peaks at 284.6 and 282.9 eV, respectively. Promotion with small amounts of boron has been reported to enhance the stability of Co FTS catalysts. To investigate the nature and location of the boron promoter on Co catalysts, calculated B 1s BEs for different possible boron species were compared with the observed B 1s XPS peak. A surface cobalt boride was found to be the most likely candidate for the XPS peak at 188.1 eV. The proposed combination of XPS and core-level BE calculations provides a powerful technique to analyze the structure of surface species and to help identify the nature and the chemical state of catalyst promoters. However, to fully characterize catalyst materials, this approach should be combined with complementary characterization techniques such as temperature-programmed reduction/oxidation, X-ray-based characterization techniques, and vibrational spectroscopy, as illustrated for the identification of resilient carbon species and a boron promotor on Co catalysts. Each of these techniques could again be combined with first-principles calculations to facilitate structural analysis.

■ ASSOCIATED CONTENT

Supporting Information

Optimized structures and the calculated core-level BEs. This material is available free of charge via the Internet at http://pubs.acs.org.

AUTHOR INFORMATION

Corresponding Author

*E-mail saeys@nus.edu.sg; Tel +65 6516 5826; Fax +65 6779 1936.

Notes

The authors declare no competing financial interest.

ACKNOWLEDGMENTS

This project is financially supported by a research grant from the Singapore Ministry of Education (R279-000-272-112). Q. T. Trinh and K. F. Tan are supported by research scholarships from the National University of Singapore.

REFERENCES

(1) Sokolowski, E.; Nordling, C.; Siegbahn, K. *Phys. Rev.* **1958**, *110*, 776.

(2) Knop-Gericke, A.; Kleimenov, E.; Havecker, M.; Blume, R.; Teschner, D.; Zafeiratos, S.; Schlögl, R.; Bukhtiyarov, V. I.; Kaichev, V. V.; Prosvirin, I. P.; et al. *Adv. Catal.* **2009**, *52*, 213−272.

(3) Venezia, A. M. *Catal. Today* **2003**, *77*, 359−370.

(4) Powell, C. J.; Jablonski, A.; Tilinin, I. S.; Tanuma, S.; Penn, D. R. *J. Electron Spectrosc. Relat. Phenom.* **1999**, *98*−*99*, 1−15.

(5) Baraldi, A. *J. Phys.: Condens. Matter* **2008**, *20*, 093001.

(6) Teschner, D.; Borsodi, J.; Wootsch, A.; Revay, Z.; Havecker, M.; Knop-Gericke, A.; Jackson, S. D.; Schlögl, R. *Science* **2008**, *320*, 86−89.

(7) Vass, E. M.; Havecker, M.; Zafeiratos, S.; Teschner, D.; Knop-Gericke, A.; Schlögl, R. *J. Phys.: Condens. Matter* **2008**, *20*, 184016.

(8) Bañares, M. A. *Top. Catal.* **2009**, *52*, 1301−1302.

(9) Tao, F.; Salmeron, M. *Science* **2011**, *331*, 171−174.

(10) Kohler, L.; Kresse, G. *Phys. Rev. B* **2004**, *70*, 165405.

(11) Siegbahn, K.; Nordling, C.; Johansson, G.; Hedman, J.; Heden, P. F.; Hamrin, K.; Gelius, U.; Bergmark, T.; Werme, L. O.; Manne, R.; et al. *ESCA Applied to Free Molecules*; North-Holland: Amsterdam, 1969.

(12) Martensson, N.; Nilsson, A. *J. Electron Spectrosc. Relat. Phenom.* **1995**, *75*, 209−223.

(13) Methfessel, M.; Fiorentini, V.; Oppo, S. *Phys. Rev. B* **2000**, *61*, 5229−5236.

(14) Weinert, M.; Watson, R. E. *Phys. Rev. B* **1995**, *51*, 17168−17180.

(15) Trinh, Q. T.; Yang, J. H.; Lee, J. Y.; Saeys, M. *J. Catal.* **2012**, *291*, 26−35.

(16) Rodriguez, J. A.; Goodman, D. W. *Science* **1992**, *257*, 897−903.

(17) Van Santen, R. A.; Neurock, M. *Molecular Heterogeneous Catalysis: A Conceptual and Computational Approach*; VCH-Wiley, Weinheim, 2006.

(18) Nørskov, J. K.; Bligaard, T.; Rossmeisl, J.; Christensen, C. H. *Nat. Chem.* **2009**, *1*, 37−46.

(19) Tielens, F.; Saeys, M.; Tourwe, E.; Marin, G. B.; Hubin, A.; Geerlings, P. *J. Phys. Chem. A* **2002**, *106*, 1450−1457.

(20) Saeys, M.; Reyniers, M. F.; Marin, G. B.; Neurock, M. *J. Phys. Chem. B* **2002**, *106*, 7489−7498.

(21) Morin, C.; Simon, D.; Sautet, P. *J. Phys. Chem. B* **2003**, *107*, 2995−3002.

(22) Olovsson, W.; Göransson, C.; Marten, T.; Abrikosov, I. A. *Phys. Status Solidi B* **2006**, *243*, 2447−2464.

(23) Takahata, Y.; Chong, D. P. *J. Electron Spectrosc. Relat. Phenom.* **2003**, *133*, 69−76.

(24) Todorova, M.; Lundgren, E.; Blum, V.; Mikkelsen, A.; Gray, S.; Gustafson, J.; Borg, M.; Rogal, J.; Reuter, K.; Andersen, J. N.; et al. *Surf. Sci.* **2003**, *541*, 101−112.

(25) Bianchettin, L.; Baraldi, A.; de Gironcoli, S.; Vesselli, E.; Lizzit, S.; Comelli, G.; Rosei, R. *J. Phys. Chem. C* **2009**, *113*, 13192−13198.

(26) Tan, K. F.; Xu, J.; Chang, J.; Borgna, A.; Saeys, M. *J. Catal.* **2010**, *274*, 121−129.

(27) Tan, K. F.; Chang, J.; Borgna, A.; Saeys, M. *J. Catal.* **2011**, *280*, 50−59.

(28) Perdew, J. P.; Burke, K.; Ernzerhof, M. *Phys. Rev. Lett.* **1996**, *77*, 3865−3868.

(29) Kresse, G.; Hafner, J. *J. Phys. Rev. B* **1993**, *47*, 558−561.

(30) Kresse, G.; Furthmuller, J. *Comput. Mater. Sci.* **1996**, *6*, 15−50.

(31) Blochl, P. E. *Phys. Rev. B* **1994**, *50*, 17953−17979.

(32) Kresse, G.; Joubert, D. *Phys. Rev. B* **1999**, *59*, 1758−1775.

(33) Weststrate, C. J.; Gericke, H. J.; Verhoeven, M. W. G. M.; Ciobîcă, I. M.; Saib, A. M.; Niemantsverdriet, J. W. *J. Phys. Chem. Lett.* **2010**, *1*, 1767−1770.

(34) Vaari, J.; Lahtinen, J.; Hautojarvi, P. *Catal. Lett.* **1997**, *44*, 43−49.

(35) Steinbach, F.; Kiss, J.; Krall, R. *Surf. Sci.* **1985**, *157*, 401−412.

(36) Lahtinen, J.; Vaari, J.; Kauraala, K. *Surf. Sci.* **1998**, *418*, 502−510.

(37) Bennich, P.; Puglia, C.; Bruhwiler, P. A.; Nilsson, A.; Maxwell, A. J.; Sandell, A.; Martensson, N. *Phys. Rev. B* **1999**, *59*, 8292−8304.

(38) Lee, A. F.; Gawthrope, D. E.; Hart, N. J.; Wilson, K. *Surf. Sci.* **2004**, *548*, 200−208.

(39) Rajumon, M. K.; Roberts, M. W.; Wang, F.; Wells, P. B. *J. Chem. Soc., Faraday Trans.* **1998**, *94*, 3699−3703.

(40) Matsumoto, Y.; Gruzdkov, Y. A.; Watanabe, K.; Sawabe, K. *J. Chem. Phys.* **1996**, *105*, 4775−4788.

(41) Freyer, N.; Pirug, G.; Bonzel, H. P. *Surf. Sci.* **1983**, *126*, 487−494.

(42) Lee, A. F.; Wilson, K. *J. Vac. Sci. Technol., A* **2003**, *21*, 563−568.

(43) Bjorneholm, O.; Nilsson, A.; Tillborg, H.; Bennich, P.; Sandell, A.; Hernnk, B.; Puglia, C.; Martensson, N. *Surf. Sci.* **1994**, *315*, L983−L989.

(44) Bondino, F.; Comelli, G.; Esch, F.; Locatelli, A.; Baraldi, A.; Lizzit, S.; Paolucci, G.; Rosei, R. *Surf. Sci.* **2000**, *459*, L467−L474.

(45) Ong, C. W.; Huang, H.; Zheng, B.; Kwok, R. W. M.; Hui, Y. Y.; Lau, W. M. *J. Appl. Phys.* **2004**, *95*, 3527−3534.

(46) Mavel, G.; Escard, J.; Costa, P.; Castaing, J. *Surf. Sci.* **1973**, *35*, 109−116.

(47) Feng, X.; Bai, Y. J.; Lu, B.; Zhao, Y. R.; Yang, J.; Chi, J. R. *Inorg. Chem. Commun.* **2004**, *7*, 189−191.

(48) Bao, K.; Yu, F.; Shi, L.; Liu, S.; Hu, X.; Cao, J.; Qian, Y. *J. Solid State Chem.* **2009**, *182*, 925−931.

(49) Berns, D. H.; Cappelli, M. A. *J. Mater. Res.* **1997**, *12*, 2014−2026.

(50) Bader, R. F. W. *Atoms in Molecules - A Quantum Theory*; Oxford University Press: New York, 1990.

(51) Henkelman, G.; Arnaldsson, A.; Jonsson, H. *Comput. Mater. Sci.* **2006**, *36*, 354−360.

(52) Zhuo, M. K.; Tan, K. F.; Borgna, A.; Saeys, M. *J. Phys. Chem. C* **2009**, *113*, 8357−8365.

(53) Zhao, H. B.; Kim, J.; Koel, B. E. *Surf. Sci.* **2003**, *538*, 147−159.

(54) Essen, J. M.; Haubrich, J.; Becker, C.; Wandelt, K. *Surf. Sci.* **2007**, *601*, 3472−3480.

(55) Mittendorfer, F.; Thomazeau, C.; Raybaud, P.; Toulhoat, H. *J. Phys. Chem. B* **2003**, *107*, 12287−12295.

(56) Brainard, W. A.; Wheeler, D. R. *J. Vac. Sci. Technol.* **1978**, *15*, 1800−1805.

(57) Mohn, P. *J. Phys. C: Solid State Phys.* **1988**, *21*, 2841−2851.